Urban Climate 51 (2023) 101663

Contents lists available at ScienceDirect

Urban Climate

journal homepage: www.elsevier.com/locate/uclim

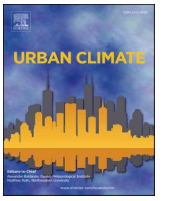

Wind and turbulence relationship with NO_2 in an urban environment: a fine-scale observational analysis

C. Román-Cascón [a,*], C. Yagüe [b], P. Ortiz-Corral [b], E. Serrano [b], B. Sánchez [b], M. Sastre [b], G. Maqueda [b], E. Alonso-Blanco [c], B. Artiñano [c], F.J. Gómez-Moreno [c], E. Diaz-Ramiro [c], J. Fernández [c], A. Martilli [c], A.M. García [d], A. Núñez [d], J.M. Cordero [e], A. Narros [e], R. Borge [e]

[a] Departamento de Física Aplicada, Facultad de Ciencias del Mar y Ambientales, INMAR, CEIMAR, Universidad de Cádiz, Puerto Real, 11510, Spain
[b] Departamento de Física de la Tierra y Asfrofísica, Universidad Complutense de Madrid, Avda. Complutense s/n, Madrid 28040, Comunidad de Madrid, Spain
[c] Department of Environment, CIEMAT, Madrid 28006, Comunidad de Madrid, Spain
[d] Department of Applied Physics and Material Engineering, Escuela Técnica Superior de Ingenieros Industriales, Universidad Politécnica de Madrid (UPM), Madrid 28006, Comunidad de Madrid, Spain
[e] Department of Chemical and Environmental Engineering, Technical University of Madrid (UPM), Madrid 28006, Comunidad de Madrid, Spain

ARTICLE INFO

Keywords:
Air pollution
Boundary-layer turbulence
Wind
Breezes
Stable conditions
AIRTEC-CM

ABSTRACT

It is well known that meteorology plays an important role in the diurnal evolution of pollutants, especially those variables related to atmospheric dispersion. Most studies typically relate the concentration of some pollutants with wind speed from conventional anemometers; however, the use of turbulence variables is less common, in part because the needed instruments are not so typical in standard air-quality stations. In this work, we compare the wind-NO_2 relationship with the turbulence-NO_2 one using observational data from two field campaigns developed in Madrid (winter and summer). The turbulence data comes from two sonic anemometers deployed at different locations: one close to the street and the other at the top of a nearby tall building. The results indicate that the turbulent variables correlate better with the pollutant concentration than the wind speed when using data from the street sonic, while the contrary is found when using the terrace sonic. These data are also used to perform a fine-scale analysis of the turbulent diffusion-NO_2 behaviour during a very-stable period in winter, when the turbulence typically shows a decrease in the evening transition, causing the highestNO_2 concentrations. Conversely, under these conditions, the formation of thermally-driven winds is also favoured later in the night, which favours the pollutant dispersion and cleaning of the air. The important role of these dynamical processes on the NO_2 evolution highlights the importance of the correct understanding of small-scale atmospheric processes to understand their relationship with the concentration of pollutants.

* Corresponding author.
E-mail address: carlos.roman@uca.es (C. Román-Cascón).

https://doi.org/10.1016/j.uclim.2023.101663
Received 7 March 2023; Received in revised form 30 June 2023; Accepted 15 August 2023
Available online 31 August 2023

1. Introduction

Air pollution has been scientifically related to negative impacts on human health, including cardiovascular (Rajagopalan et al., 2018), immune (Glencross et al., 2020), oncological (Raaschou-Nielsen et al., 2013), or psychiatric (Bernardini et al., 2020) effects. This is especially relevant in cities (Mayer, 1999), leading to a significant majority of the global population (>99%) exposed to pollutant levels exceeding the most recent World Health Organization (WHO) guideline limits (WHO, 2021).

The analysis of the different agents that control the concentration of pollutants in cities is key for a better adaptation to these dangerous situations, as well as for the development of better strategies for air pollution mitigation (Harlan and Ruddell, 2011). Keeping in mind the importance of the variability in pollutants emissions and their chemical reactivity, the role of meteorology on their final concentration observed close to the surface has been widely recognised through scientific studies carried out with diverse approaches.

Some studies have addressed the effect of climatological changes on air quality by investigating future conditions with climate models, as in Westervelt et al. (2016), who focused on the O_3 concentration at the global scale. Others have analysed changes in past climatological conditions attending to observations in more limited areas, as for example in Querol et al. (2014), who analysed trends on pollutant levels during a decade in Spain, or Borge et al. (2019), who extended the strategy for several pollutants during 25 years. In some of these studies, the concept of weather penalty is also introduced (Jhun et al., 2015), which states that the effects of control policies applied in the emission of some pollutants can be partially dampened due to changes in the atmospheric conditions.

Hence, it is also useful to analyse how these pollutants behave at specific locations within smaller time scales. This is done, for example, in Patra et al. (2008) or Borge et al. (2016), among others. These studies need to take into account the effect of emissions, chemical reactivity, and those related to the changes in meteorological conditions during the observational period. Observationally, it is common to investigate the meteorology-pollutant relationships using the wind as a variable related to atmospheric diffusion (Donnelly et al., 2011), especially for some pollutants like NO_2, one of the most dangerous gases for human health and the focus of this study. In other cases, the analysis of the synoptic conditions or other meteorological variables is also considered (Grundström et al., 2015; Laña et al., 2016). Regarding the turbulence effect in the lower atmosphere, although the literature is rich in analytical and modelling studies through diverse approaches (e.g., Vilà-Guerau De Arellano and Duynkerke, 1992; Lateb et al., 2016; Santiago et al., 2020; Martilli et al., 2021; Li et al., 2021), there is a lack of observational studies that include in-situ (real) turbulence data concerning the concentration of pollutants in cities. This is - in part - due to the difficulties associated with the calculation of reliable turbulent parameters from observational measurements in urban environments. However, these studies are needed to better understand how the pollutants behave at the micro-scale level (<1 km), which is crucial for future urban management plans and to design more appropriate strategies for pollutants-effect mitigation (Fernando et al., 2010).

The objectives of this paper are tied to this necessity and are listed hereinafter. The first objective tries to determine whether the turbulent parameters calculated from sonic anemometers add valuable information for the dispersion of pollutants in comparison with the more commonly used 2D wind speed measurements. The second objective is focused on of the pollutant-meteorology relations found among two sonics, one installed close to the street level and the other over the terrace of a tall building, taking into account their different exposure to urban obstacles. Finally, the third objective is to investigate the micro and mesoscale atmospheric processes developed during a period characterised by high NO_2 concentration. These processes include the investigation of how the turbulence decays during the afternoon and evening transition or the nighttime development of thermally-driven flows. Despite the open discussion and the exposed limitations of the analyses here presented, we hope that the results shown in this paper can help to better understand the complex small-scale processes that sometimes lead (or not) to high pollutant concentrations. These aspects are difficult to be investigated with larger-scale data, mesoscale models, or even with higher-resolution models.

The paper is structured as follows: Section 2 describes the emplacement, the instruments, and the methodologies used to prepare and analyse the data. In Section 3, we present and discuss the results, organised from the larger-scale point of view to the most detailed analyses of small-scale processes. Section 4 is included to discuss some of the results and limitations of the study and a summary and the main conclusions are presented in Section 5.

Table 1
Summary of the instruments used in the study, including some technical information. The variables u, v, w, and T correspond to the three components of the wind and the atmospheric temperature. TKE, u_*, WS, WD, SH correspond to turbulent kinetic energy, friction velocity, wind speed, wind direction, and sensible heat flux, respectively. NO_2 is the nitrogen dioxide concentration.

Instrument	Raw variables (processed)	Freq. sampling (averaging)
Sonic anemometer	u, v, w, T	10 Hz
(terrace)	(TKE, u_*, WS, WD, SH)	(10 min)
Sonic anemometer	u, v, w, T	20 Hz
(street)	(TKE, u_*, WS, WD, SH)	(10 min)
Air-quality station		1 min
(Castellana-Madrid)	NO_2	(10 min)
Traffic counter		1 h
(Castellana-Madrid)	Traffic intensity	(10 min)

2. Data and methodology

2.1. The AIRTEC-CM field campaigns

The *Urban Air-Quality and Climate-Change Integral Assessment* project (AIRTEC-CM) included the development of different urban field campaigns in the city of Madrid to reach some of its main scientific objectives (Cordero et al., 2021). One of these objectives was to deepen on the study of the pollutants-meteorology relationships, which is the aim of this paper. In this work, we have used data from two of these campaigns developed around the area of the School of Industrial Engineering (40°26'25" N; 3°41'22" W). The site is close to *Castellana* Street, which is a very popular street in Madrid normally characterised by constant and relatively high traffic intensity during the daytime, peaking in the morning and afternoon because of the routine commuting. We focus on the periods comprising all days from 13 to 25 February 2020 (winter field campaign) and from 17 June to 04 July 2021 (summer field campaign). Several instruments were installed during these periods to measure different variables, including both the concentration of pollutants and the meteorological conditions (Table 1).

Among the meteorological instrumentation deployed, we focus on two sonic anemometers installed at nearby but different emplacements (Fig. 1). Subsequently, these sonics will be referred to as the *Street* and *Terrace* sonic.

The Street sonic (Young 81,000) was installed over the air-quality station used, a small building of 2.5 m height (total height of 5.5 m above the street level, see Fig. 1). The Terrace sonic (Irgason, Integrated CO_2 and H_2O Open-Path Gas Analyzer and 3-D Sonic Anemometer) was installed on the terrace of a larger building of 22 m height (total of 26 m above the street level, see Fig. 1).

The Street sonic was much more perturbed due to the obstacles surrounding the area, but just above the device measuring the NO_2 concentration (air-quality station), while the Terrace sonic was over a less perturbed area, but 26 m higher than the street level where the pollutants were measured.

The NO_2 measurements were obtained from the *Castellana* air-quality station. It is a fixed air-quality station belonging to the Madrid City Council network, considered as a *traffic* station since it is close to an important street (*Castellana* street) of Madrid. However, it does not typically reach very high pollutant levels from traffic emissions in comparison to other air-quality stations in the city since it is installed at a relatively calm park surrounded by some trees and buildings. This station measures PM 2.5, PM 10 and the nitrogen oxides (NO_2, NO, NO_x) based on chemiluminescence. Additionally, the *Castellana*-street traffic intensity data (vehicles/h) from the Madrid City Council was also employed in this work to take into account their effect on the NO_2 concentration levels.

2.2. Procedures applied to the sonics anemometers

The procedures applied to the sonic anemometers were identical for both instruments, taking into account their different sampling frequency (10 Hz for the Terrace sonic and 20 Hz for the Street sonic). We used the high-frequency raw data from the sonics (the three components of the flow and the temperature) to calculate different variables that are used in the article: wind speed (WS), wind

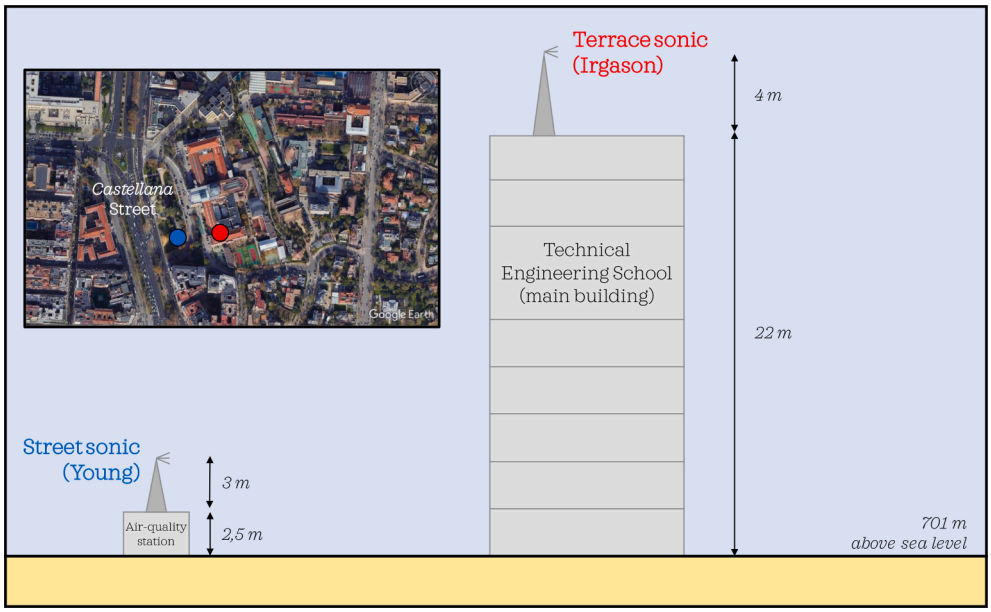

Fig. 1. Google Earth satellite image of the area studied (inner box), including the location of the two sonics with blue (Street sonic) and red (Terrace sonic) markers. The illustration shows the heights and distances needed to understand the differences between the two emplacements. Note the Street sonic was installed over the air-quality station building. Both emplacements were separated around 60 m horizontally. (For interpretation of the references to colour in this figure legend, the reader is referred to the web version of this article.)

direction (WD), turbulent kinetic energy (TKE, Eq. (1)), friction velocity (u_*, Eq. (2)), and sensible heat flux (SH, Eq. (3)). Two main techniques are employed: the eddy covariance (EC, Stull, 1988) using 10-min averaging windows and the Multi-resolution flux decomposition (MRFD; Howell and Mahrt, 1997), both extensively described in the literature.

$$\mathrm{TKE} = \frac{1}{2}\left(\overline{u'^2} + \overline{v'^2} + \overline{w'^2}\right) \quad , \tag{1}$$

$$u_* = \sqrt[4]{\left(-\overline{u'w'}\right)^2 + \left(-\overline{v'w'}\right)^2} \quad , \tag{2}$$

$$\mathrm{SH} = \rho c_p \quad \overline{\theta' w'} \quad , \tag{3}$$

where u', v', w' are the fluctuations of the three components of the flow, θ' is the fluctuation of the potential temperature, ρ is the air density, and c_p is the air specific heat at constant pressure.

The comparison between TKE and u_* is included in this article because u_* mainly includes the mechanical turbulence due to wind shear (covariances of the horizontal components of the flow, linked to wind shear, see Eq. (1)) while TKE also comprises the influence of the thermal turbulence or convection (variance of the vertical component of the flow (w', see Eq. (2))). While both variables typically show a similar behaviour, they can differ in some cases, especially in those in which convective conditions are more important.

We have checked the effects on the results of applying rotation (double-rotation and planar-fit rotation) and high-pass filtering (5 min) to the raw data before calculating the final EC and MRFD values. Although some divergences exist, the results and conclusions obtained with the different possible options (none, rotation, high-pass filter, or both) are not very different. Hence, the results shown in the paper are those obtained without the application of rotation to the raw sonic data and without filtering the low-frequency (high-pass) signal of the data. The analysis of the results obtained using the different pre-processing techniques is interesting to investigate the effect of some processes of different scales under some specific conditions. However, this comparison deserves a fully-dedicated study and it is out of the scope of the present work.

2.3. Performance scores

Threshold values of WS, TKE, or u_* are calculated in Section 3.2 to be associated with NO_2 concentrations. Specifically, we analyse the skill of expecting high NO_2 concentration (namely, higher than 125 μg m^{-3}) when the meteorological variables are lower than selected threshold values (using 10-min data). To do it, we define a contingency table (Table 2) that is used to calculate three performance scores based on the classical forecast score parameters: the hit rate (HR; Eq. (4)), the false-alarm rate (FA; Eq. (5); Barnes et al. (2009)), and the Gilbert skill score (GSS; Eq. (6); Schaefer (1990)).

$$\mathrm{HR}(\%) = \frac{a}{a+c} \times 100 \quad , \tag{4}$$

$$\mathrm{FA}(\%) = \frac{b}{b+d} \times 100 \quad , \tag{5}$$

$$\mathrm{GSS} = \frac{a - a_r}{a+b+c-a_r} \quad , \tag{6}$$

where a_r is:

$$a_r = \frac{(a+b)(a+c)}{a+b+c+d} \quad . \tag{7}$$

The HR focuses on the percentage of times that the meteorological variable is lower than the threshold with respect to all the times when the NO_2 concentration is higher than 125 μg m^{-3}, which is similar to a correct forecast. The FA focuses on the percentage of times that the NO_2 concentration is lower than 125 μg m^{-3} but the variable is still lower than the threshold, similar to a false alarm. The GSS is also known as the Equitable Threat Score, being a better balanced score which includes aspects from both the HR and the FA. It is also an appropriate score for rare events since it does not deteriorate the performance when the events are not very common in long time series (as is the $NO_2 > 125$ μg m^{-3}). This is useful for studies of rare events such as tornadoes or fog (Román-Cascón et al., 2016). Its minimum value is near 0 and reaches 1 for perfect forecasts.

Table 2
Classical score parameters as applied in this work, where the variable can be wind speed (WS), turbulent kinetic energy (TKE), or friction velocity (u_*). The threshold values are explored in Section 3.2.

WS, TKE, u_*	$\mathbf{NO_2} > 125$ μg m^{-3}	$\mathbf{NO_2} < 125$ μg m^{-3}
variable < threshold	a (hit)	b (false alarm)
variable > threshold	c (miss)	d (correct rejection)

Note how in this work we use observed meteorological values, which allows the analysis of the skills of the different variables and the selection of specific thresholds. Potentially, the use of forecasted meteorological values could be useful for air-quality forecasting purposes, although this application deserves fully dedicated research efforts that are out of the scope of this article.

3. Results

3.1. Overview of the winter and summer field campaigns

An overview of the wind and turbulence (TKE) evolution during the winter and summer field campaigns is shown in Fig. 2, with the NO_2 concentration with coloured symbols. For the sake of clarity, only the Terrace sonic is shown in all figures of the article, except when the objective is to compare both sonic anemometers. The figures obtained with the Street sonic are shown in the supplemental material. A quick visual analysis of Fig. 2 reveals how the concentrations reached during the winter field campaign were notably higher than those observed during the summer one. This was mainly associated with the weaker wind speed and turbulence during the winter field campaign (also observed in Table 3). Some nighttime periods in the summer field campaign displayed wind speed lower than 1 m s^{-1} and TKE lower than 0.5 m^2 s^{-2} (Fig. 2b, d). However, the enhanced turbulence during the daytime in summer (see high TKE peaks in Fig. 2d) avoided reaching high concentrations of NO_2 during the calmer night periods. The enhancement of atmospheric diffusion due to the convective thermals in summer helped to reduce the NO_2 concentration. This effect was added to the favoured conversion from NO_2 to ozone due to the increase in UV radiation. In contrast, the daytime maxima values of TKE during the winter field campaign (Fig. 2c) were notably lower due to the limited convection in wintertime. This prevented the diffusion of NO_2 and allowed higher concentrations during the daytime, but especially throughout the first hours of the night.

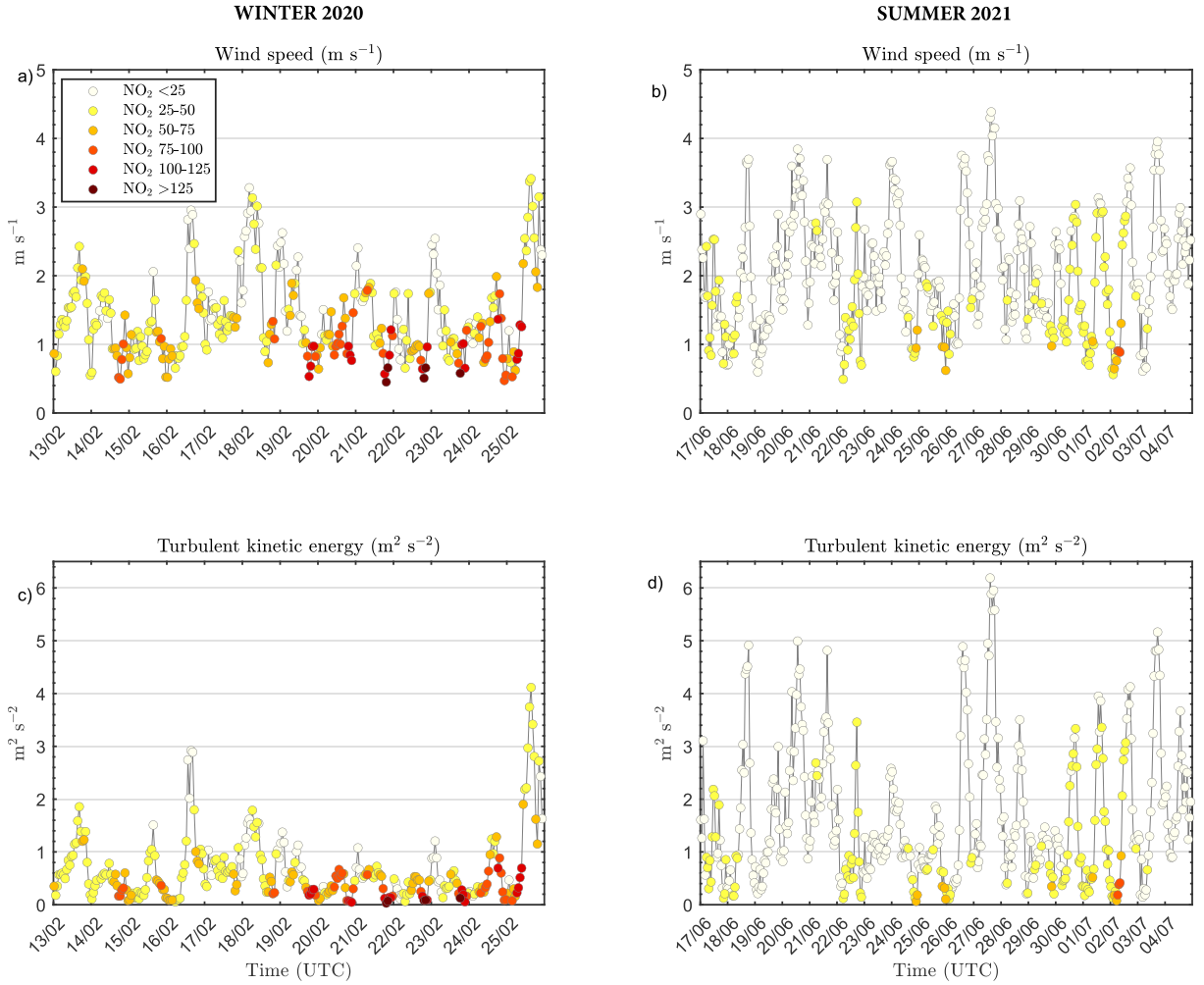

Fig. 2. Overview of the winter 2020 (left panels) and the summer 2021 (right panels) AIRTEC-CM field campaigns: wind speed (m s^{-1}, upper panels) and TKE (m^2 s^{-2}, bottom panels) from the Terrace sonic. The NO_2 concentration is included in μg m^{-3} with coloured symbols, see legend in panel a. All values shown are hourly averages. The same figure but using data from the Street sonic is included in Fig. S2 of supplemental material.

Table 3
Values of statistical parameters (mean, standard deviation and maximum value) based on 10-min data of the NO_2 concentration ($\mu g\ m^{-3}$), wind speed ($m\ s^{-1}$), TKE ($m^2\ s^{-2}$), u_* ($m\ s^{-1}$), and SH ($W\ m^{-2}$) during the field campaigns. Meteorological data from the sonic installed at the terrace. The same table with measurements from the Street sonic data is included in Table S3 of supplemental material.

Terrace sonic	NO_2	Wind speed	TKE	u_*	SH
	Mean (Std) (Max)	Mean (Std)	Mean (Std)	Mean (Std)	Mean (Std)
Winter 2020	50.2 (29.7) (163)	1.39 (0.68)	0.65 (0.69)	0.30 (0.17)	29.18 (53.99)
Summer 2021	20.4 (13.4) (100)	2.00 (0.90)	1.60 (1.34)	0.55 (0.29)	122.55 (153.68)

3.2. NO_2 concentration relationship with wind speed, TKE, and u_*

The first question addressed in this study is devoted to investigating whether the NO_2 concentration correlates better with the wind speed or with some turbulent parameter that includes the vertical velocity component of the flow. Hence, we focus on the comparison of NO_2 concentration correlation with wind speed, TKE, and u_*. For the correlation (linear Pearson) calculation, the logarithm of the meteorological value is used, due to the exponential growth of NO_2 concentration with low values of wind speed, TKE, and u_*. In this regard, the conclusions obtained with the linear values are similar, but the correlations are larger using the logarithmic one. Due to the difficulty to measure reliable and representative values of wind and turbulence in complex urban areas, the second question of the study tries to explore whether the differences in these relations are conserved when using data from sonic anemometers deployed at different emplacements: terrace and street, described above in Section 2.

Fig. 3 shows the correlation obtained using all the available possibilities to answer the two previous questions. The results are separated for the summer and winter field campaign, as well as for a shorter period of three days (21, 22, and 23 of February 2020). These days were selected because the highest NO_2 concentrations were observed, associated with a synoptically-stable period (see Figs. 2a,c). The comparison among the periods reveals how the correlations were similar for both seasons, although with a slightly better relationship of the meteorological variables and NO_2 in winter than in summer (Fig. 3), with remarkably better relationship during the stable period of winter (Fig. 3 panel c).

The turbulence- NO_2 correlation was larger (in absolute value) than the wind speed- NO_2 one when using the Street sonic for all the studied periods, especially when using the friction velocity. If the NO_2 concentration is used as a passive tracer of the atmospheric turbulence, this indicates how the turbulence measurements taken at the street level include valuable information (vertical component of the flow) to relate to the atmospheric diffusion that impacts directly the NO_2 concentration, despite the city obstacles at this level. However, the contrary was found when using data from the Terrace sonic, with larger correlation (in absolute value) for the wind speed- NO_2. In this case, the turbulence measured at 26 m agl was somehow de-coupled from the street diffusion, worsening the correlations, except during the stable period of winter, when the TKE shows a similar correlation than the wind speed.

3.3. NO_2 prediction using wind and turbulence measurements

The correlations found are not high enough to establish a unique relationship between NO_2 and the meteorological variable (due to the different aspects involved in the NO_2 evolution (emissions, advection, chemical reactions, etc.), some of which are commented in Section 4. However, from a predictive point of view, it is still interesting to determine statistically the wind/turbulence values

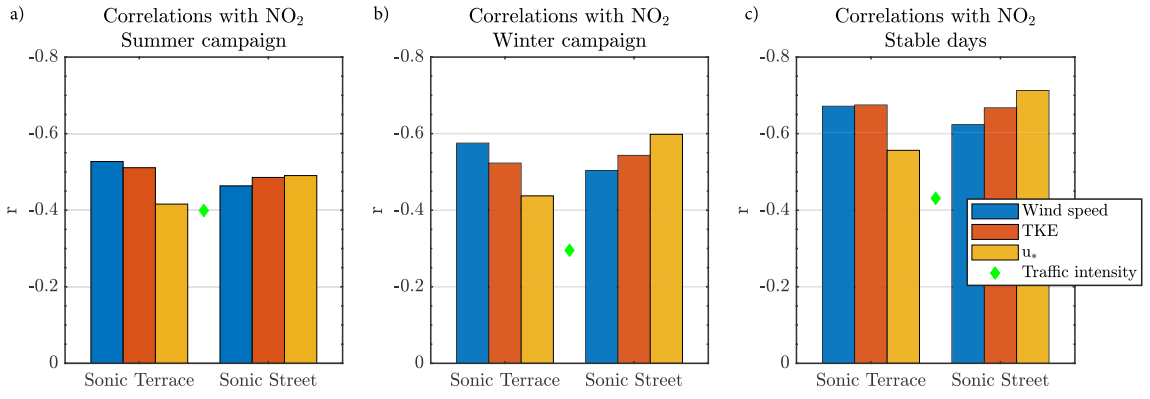

Fig. 3. Pearson correlation of NO_2 concentration (10-min data) with different variables measured at the terrace and street levels for the summer and winter field campaigns (a and b, respectively) and for the synoptically-stable period with the higher NO_2 concentrations (21, 22, and 23 of February 2020) (c). Variables from sonic anemometers are: wind speed in blue, turbulent kinetic energy (TKE) in red, and friction velocity (u_*) in orange. The correlation with the traffic intensity data is indicated in both campaigns with a green diamond (note it corresponds to the correlation with the sign changed, since the correlation between NO_2 and traffic is positive). All 10-min time series have been smoothed using a 1-h running mean to avoid extreme peaks. (For interpretation of the references to colour in this figure legend, the reader is referred to the web version of this article.)

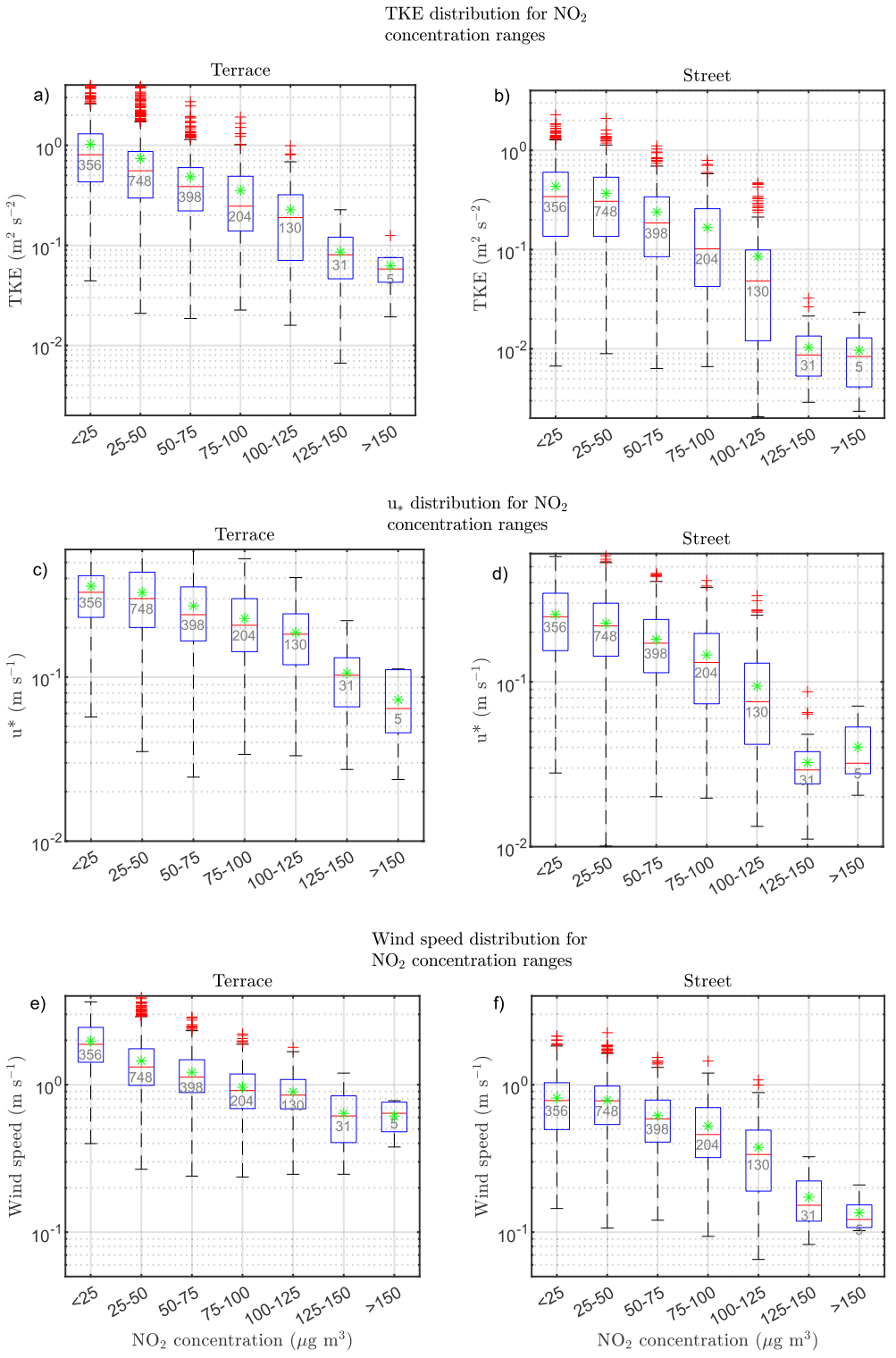

Fig. 4. TKE (upper panels), u_* (middle panels), and wind speed (bottom panels) data distribution (boxplots) associated with different NO_2 concentration ranges (x-axis) for the Terrace (left) and the Street (right) sonic anemometers using data from the winter field campaign. The box in each plot indicates the 50% of data around the median value (red line inside) in the distribution, the whiskers indicate the remaining 25%, the outliers are indicated with red crosses and mean values are indicated with green stars. Grey numbers inside the box indicate the number of data used in each range. The winter field campaign has been considered. (For interpretation of the references to colour in this figure legend, the reader is referred to the web version of this article.)

associated with the different NO_2 concentrations. This is linked to the predictive capacity of these variables, for example using forecasts from numerical weather prediction (NWP) models output. Indeed, the previous results indicated that these relationships are more important during periods characterised by stable conditions (Fig. 3c), which are the most interesting ones due to their typical association with high NO_2 concentration. This opens a new question focused on whether we can determine some wind or turbulence threshold value to be associated with high NO_2 concentration. In this sense, Fig. 4 shows the statistical distribution of TKE, u_*, and wind speed for different NO_2 concentration ranges, both using the Street and the Terrace sonics for the winter field campaign. Note how, subsequently, we focus on this campaign due to the absence of high NO_2 concentrations during the summer one (see Fig. 2).

The 10-min data distributions of TKE, u_*, and wind speed display a decreasing tendency on their values with increasing NO_2 concentrations (Fig. 4). Besides, the distributions for the Street sonic (right panels) associated with high NO_2 concentrations (especially $>125\ \mu g\ m^{-3}$) seem to shift towards more extreme values than the ones at the terrace (left panels). This motivates the quantification of the predictive skill of these variables to be associated with high NO_2 concentration. That is, we have checked if a threshold value of TKE, u_* or wind speed could be used as an indicator of high NO_2 concentration ($> 125\ \mu g\ m^{-3}$), which could have a potential interest for pollutant forecasting.

Different threshold values of the meteorological variables can be extracted from the distributions shown in Fig. 4. In this case, we focus on the maximum values corresponding to the percentiles 75 (upper line of the blue boxes) and 50 (median, red line within the blue boxes) of the distributions associated with NO_2 concentration $>125\ \mu g\ m^{-3}$ (the two boxplots more to the right in each panel of Fig. 4). These values are indicated in Table 4, together with their results for the hit rate, false alarm ratio, and Gilbert Skill Score (see Section 2). Logically, using the median as a threshold parameter worsens the hit rate and improves the false alarm ratio in comparison to the use of the 75th percentile (since P50 < P75 the TKE, u_*, or WS median values are lower than the percentiles 75). In any case, from Table 4 we can clearly conclude that the variables from the Street sonic have much better skill (lower FA for similar HR), especially using the turbulent parameters (TKE using P75 and u_* using the P50, whose respective GSS are marked in bold in the table).

Certainly, the selection of the best options will depend on the forecaster's purposes; for example, using the percentile 75 for u_* (a value of 0.05 m s^{-1}) will lead to up to 88.9% of hit rate using the Street sonic data with only 7.19% of FA. That is, with this threshold value, we would provide successful forecasts of NO_2 higher than $125\ \mu g\ m^{-3}$ with a probability of almost 90% of the times, at a cost of false alarm ratio of around 7%.

The balance between high HR and low FA, as well as the rest of possibilities are somehow included in the GSS, which also takes into account the full size of the sample, being a very appropriate performance score for rare events such as the highly polluted episodes here studied. Hence, GSS as a performance score has been optimised (maximised) in Table 5 to provide the best thresholds to be used. In this case, again the TKE and u_* calculated from the sonic situated at the street level were the two variables with better results. The evolution of the scores depending on the threshold values is shown in Fig. 5 for both sonics. In general, the results obtained with the Street sonic were better than those from the Terrace sonic (lower FA and larger HR and GSS), aspect that can be also attributed to the closeness of this sonic to the air-quality station. As an extreme case, HR of 100% can be obtained at the expense of only 10% of FA when using a TKE threshold of around 0.032 $m^2\ s^{-2}$ (Fig. 5d).

3.4. The stable period with higher NO_2 concentrations (19 to 24 Feb 2020)

The highest NO_2 concentrations during the two analysed field campaigns were observed throughout the evening transition and first hours of the night of the period comprising from 19 to 24 of February 2020 of the winter field campaign (Fig. 6). These days were

Table 4
Hit rate (HR), false alarm (FA), and Gilbert Skill Score (GSS) of expected high NO_2 concentration (i.e., $>125\ \mu g\ m^{-3}$) obtained when using a threshold value (< =) of TKE, u*, and WS. The threshold value is the 75th percentile of the data distribution shown in Fig. 4 (the maximum value between the two last boxplots (125–150 and $> 150\ \mu g\ m^{-3}$)). The winter field campaign has been considered. The same calculation is presented below for the 50th percentile (median). Most relevant values marked in bold.

75th percentile	HR (%)	FA (%)	GSS	Threshold value
TKE - Terrace	75.00	10.84	0.10	0.121 $m^2\ s^{-2}$
u* - Terrace	77.78	12.31	0.09	0.131 m s^{-1}
WS - Terrace	77.78	19.06	0.06	0.840 m s^{-1}
TKE - Street	75.00	3.70	**0.25**	0.013 $m^2\ s^{-2}$
u* - Street	88.89	7.19	0.18	0.053 m s^{-1}
WS - Street	77.78	6.92	0.16	0.222 m s^{-1}

50th percentile	HR	FA	GSS	Threshold value
TKE - Terrace	55.56	5.83	0.12	0.081 $m^2\ s^{-2}$
u* - Terrace	52.78	6.97	0.10	0.103 m s^{-1}
WS - Terrace	55.56	7.41	0.10	0.640 m s^{-1}
TKE - Street	52.78	1.85	0.26	0.009 $m^2\ s^{-2}$
u* - Street	63.89	2.40	**0.28**	0.032 m s^{-1}
WS - Street	55.56	2.23	0.25	0.152 m s^{-1}

Table 5
Idem, but with the values based on the optimization (maximum) of the Gilbert Skill Score (GSS) obtained for all possible percentiles.

Optimised values	HR	FA	GSS	Threshold value
TKE - Terrace	38.89	2.18	0.17	0.053 $m^2\ s^{-2}$
u* - Terrace	30.56	2.18	0.13	0.066 $m\ s^{-1}$
WS - Terrace	30.56	1.80	0.15	0.446 $m\ s^{-1}$
TKE - Street	**38.89**	**0.49**	**0.30**	**0.006** $m^2\ s^{-2}$
u* - Street	63.89	2.40	0.28	0.032 $m\ s^{-1}$
WS - Street	36.11	0.65	0.26	0.125 $m\ s^{-1}$

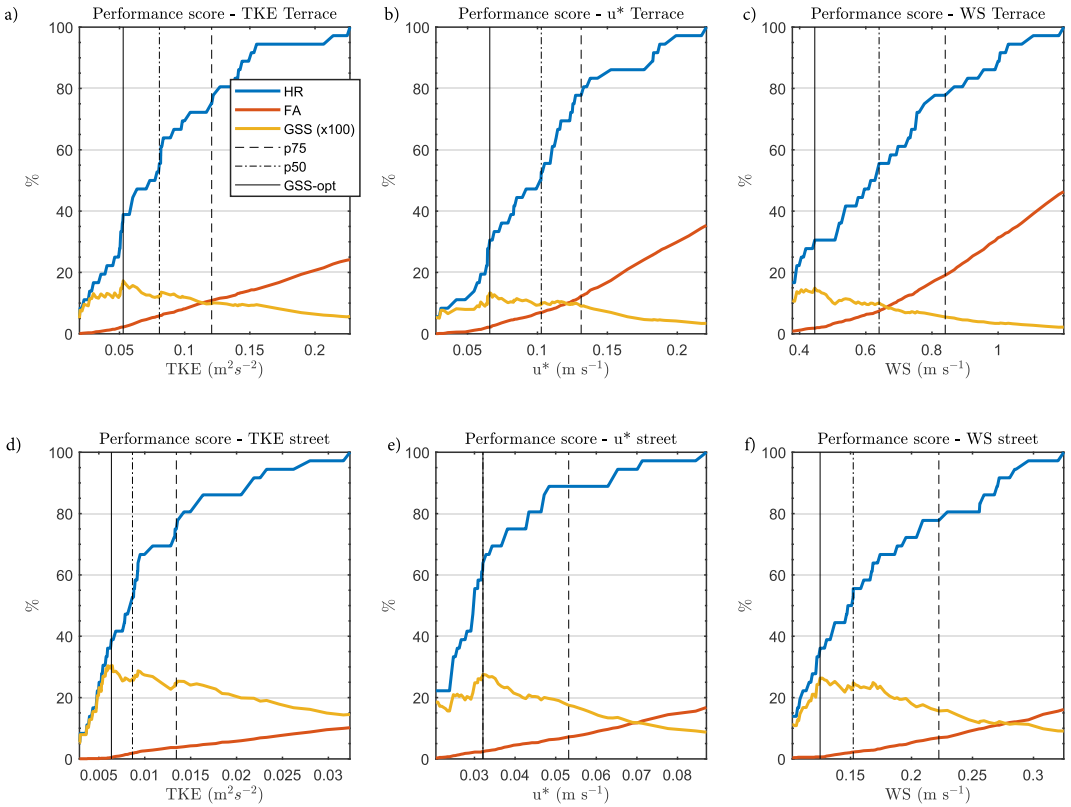

Fig. 5. Variation of the performance scores as a function of the values of TKE (left panels), u* (middle panels) and WS (right panels) used as the threshold in their computation (Eqs. (4–6)) to quantify the skill of expected high NO_2 levels. Data from the terrace (upper panels) and the street (bottom panels) sonics. The performance scores analysed are hit rate (HR, blue lines), false alarm ratio (FA, red lines), and the Gilbert Skill Score (GSS (multiplied by 100), yellow lines). The vertical lines indicate the values for percentile 75 (dashed line), percentile 50 (dashed-dotted line), and the value for the maximum GSS (solid line). The winter field campaign has been considered. (For interpretation of the references to colour in this figure legend, the reader is referred to the web version of this article.)

characterised by a high-pressure blocking system situated over western Europe, with a weak surface-pressure gradient in the central area of the Iberian Peninsula (not shown). This situation favours very low wind conditions, especially during the evening transitions, which were the periods with highest NO_2 concentrations (Fig. 6a).

Conversely, these days also showed a rapid decrease in NO_2 concentration up to remarkable minimum values around midnight (Fig. 6c), related to the enhancement of thermally-driven breezes. These mesoscale winds are also favoured under synoptically stable conditions (weak pressure gradients and clear skies) and are manifested by a typical wind-direction reversal twice per day (morning and evening). In the cases here analysed, the evening reversal was observed around 22:00 UTC, with NE winds reaching their maxima intensities after midnight (Fig. 6a). This caused important reductions in the NO_2 concentration, just a few hours after the highest concentrations were typically observed.

The percentage of time with NO_2 concentrations larger than 25 or 50 $\mu g\ m^{-3}$ from 00:00 to 04:00 UTC during the stable days (with enhanced breezes) was smaller than those found during the less-stable days (Fig. 7 panel a), despite the larger concentrations observed during the previous hours (from 16:00 to 23:00 UTC) during the stable days (Fig. 7b). Although the complex topography can in some cases add especially negative factors towards poor air quality (e.g., cities in cold pools), in this case, the contrary is observed. The

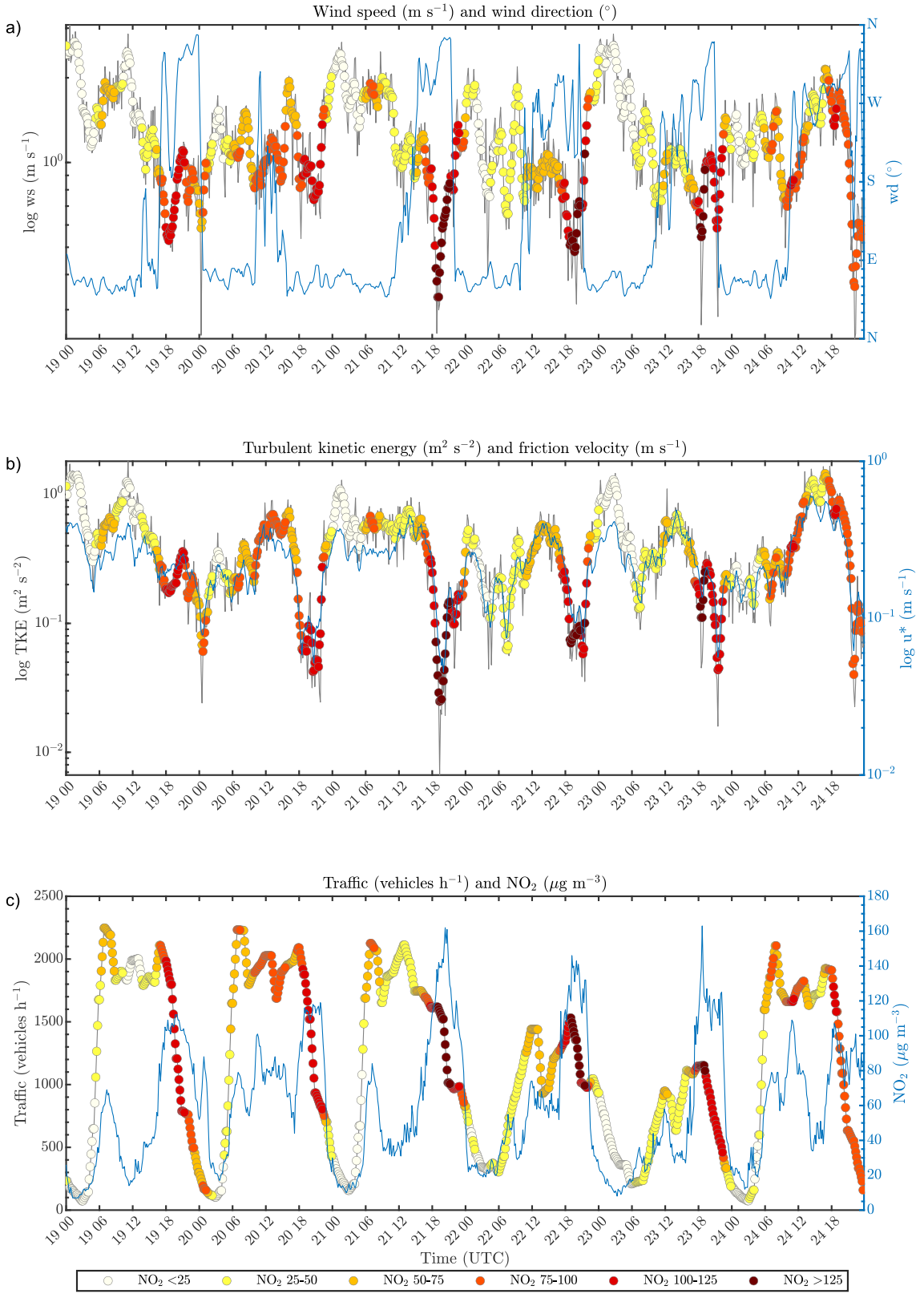

(caption on next page)

Fig. 6. The synoptically-stable period, from 19 to 24 February 2020: a) Wind speed (ms^{-1} with colours of the symbols indicating the NO_2 concentration) and wind direction (° from North, blue line); b) Turbulence kinetic energy (TKE, $m^2\ s^{-2}$, with colours of the symbols indicating the NO_2 concentration) and friction velocity (u_*, m s^{-1}, blue line); c) Traffic intensity (vehicles/h, with colours of the symbols indicating the NO_2 concentration) and the time series of the NO_2 concentration ($\mu g\ m^{-3}$, blue line). Wind speed and TKE plotted with logarithmic y-axis, using 10-min data in the grey lines and a 1-h running mean in the coloured symbols signal, for a better visualization. The NO_2 concentration indicated with colours is expressed in $\mu g\ m^{-3}$, see legend. All meteorological variables from the sonic anemometer at the terrace. The same figure with the Street sonic is included in Fig. S6 of supplemental material. (For interpretation of the references to colour in this figure legend, the reader is referred to the web version of this article.)

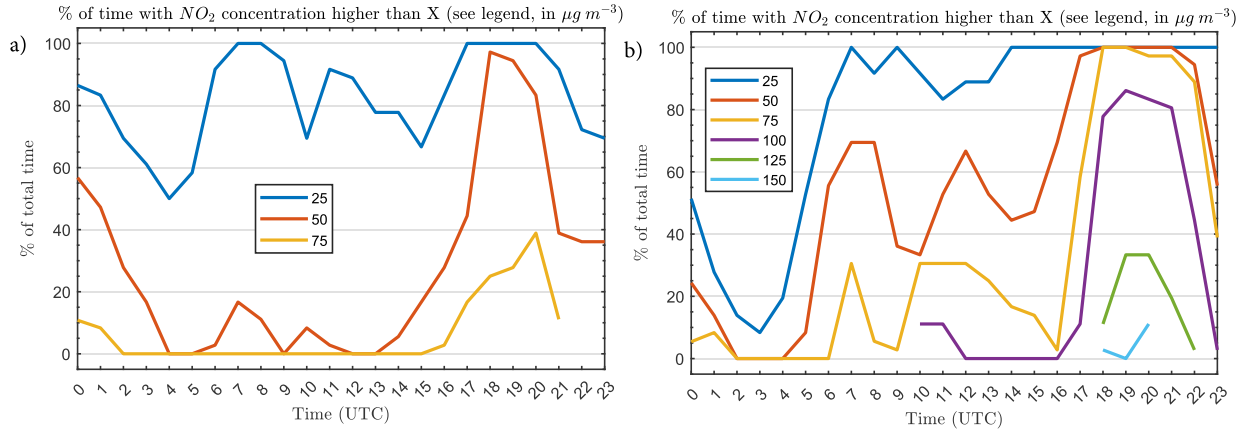

Fig. 7. Percentage of time from total for each hour of the day with NO_2 concentration higher than X (value shown with colours and indicated in the legend, in $\mu g\ m^{-3}$) for the period comprising 13–18 (both included) February 2020 (a, the less stable period), and 19 to 24 (both included) February 2020 (b, the stable period).

topography-generated flows favoured the air cleaning in situations that otherwise could be critical even during the nighttime, highlighting the relevance of these mesoscale winds for the air quality of the city.

As observed in Fig. 6 and Fig. 7, the NO_2 concentrations higher than 125 (and even 150) $\mu g\ m^{-3}$ were always observed between 18:00 and 22:00 UTC, coinciding with the near-calm period of the evening transition, with weak wind speed generally lower than 1 m s^{-1}. However, despite that the wind speed reached values lower than 1 m s^{-1} during the 6 days analysed in Fig. 6, only 3 of them showed NO_2 concentrations larger than 125 $\mu g\ m^{-3}$, which motivates studying the factors that favoured (or not) the high concentrations through the comparison among days.

The wind speed during the afternoon/evening transition of the 6 days of the stable period is shown differently in Fig. 8. These days were similar in terms of the synoptical situation, with similar radiative characteristics (clear skies), displaying only a slight gradual increase in temperature from day 19 to 24 (not shown), hence being comparable to detect influences from micrometeorology. The mean of different variables for each of the days is also summarised in Table 6 for the afternoon (12:00 to 18:00 UTC) and evening (18:00 to 21:00 UTC) periods.

On the one hand, the general behaviour of days 21, 22 and 23 (the days with NO_2 concentration higher than 125 $\mu g\ m^{-3}$) was similar, with wind speed around 1 m s^{-1} during the afternoon and decreasing soon before the sunset, reaching values below 0.5 m s^{-1}. On the other hand, the days 19, 20 and 24 (those days without NO_2 concentration higher than 125 $\mu g\ m^{-3}$) presented slightly different, but important, values (Fig. 8 and Table 6).

For the day 24 of February, the wind speed was stronger during the afternoon hours, avoiding very high NO_2 concentration during the night, despite the stabilization observed around 22:00 UTC (see Fig. 8, light-blue line). Similarly, the wind-speed maxima values observed during the afternoon hours (12:00 to 18:00 UTC) of the days 19 and 20 (blue and green lines in Fig. 8), seemed enough to diffuse the pollutants in the air during the daytime, avoiding higher NO_2 concentration during the first hours of the nighttime (18:00 to 21:00 UTC), despite the decrease in wind speed after the sunset. Hence, although the evening stabilization, characterised by an important decrease in the turbulence and wind speed values, is needed to reach very low NO_2 concentrations, the wind speed reached during the daytime (afternoon) seems also crucial for the diffusion of pollutants before the evening highest concentrations. Something similar was found in the previous section through the comparison of the summer and the winter field campaigns, with diminished NO_2 concentration maxima in part due to the enhanced convective turbulence during the daytime in summer (Fig. 2d).

The wind speed shown in Table 6 suggests that the afternoon values have an even more important role to reach high NO_2 concentration than the evening ones, while the same is not observed for the TKE or u_*. That is, the u_* afternoon values for the days with the highest pollutant levels were even larger than other days with less NO_2 concentration. This agrees with the results shown in Fig. 3b,c and highlights again how the turbulence measured at the terrace level was somehow less coupled to the NO_2 concentrations than the wind speed measured at this emplacement. However, at the street level, the turbulence seemed more related to the NO_2 concentrations reached (see values shown in Table S6 of supplemental material), as also observed in Fig. 3b,c.

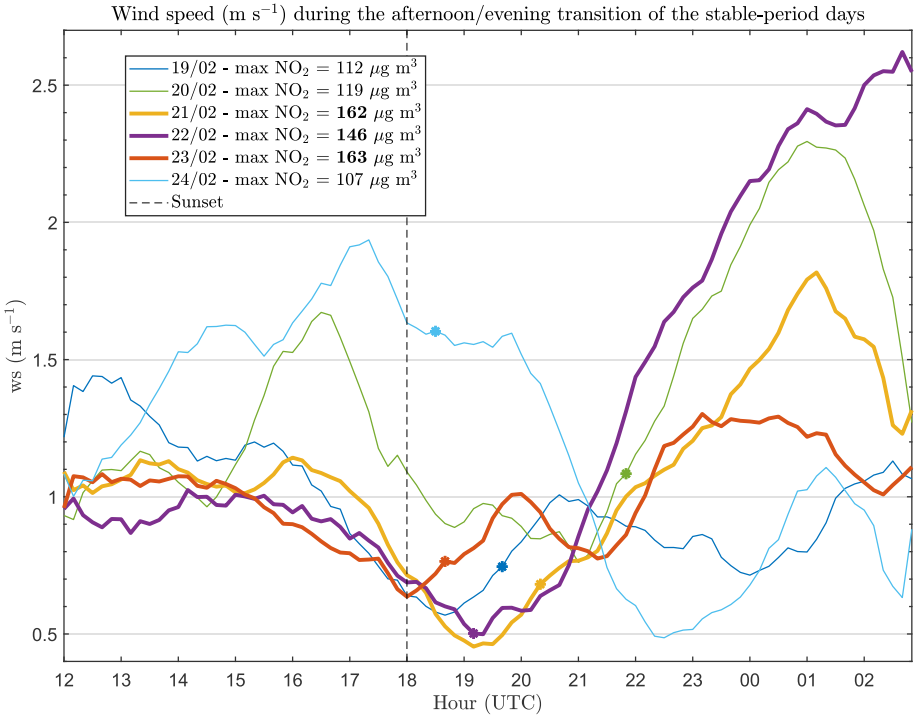

Fig. 8. Wind speed (m s^{-1}) during an extended period of the afternoon/evening transition of the days 19 to 24 February 2020 (stable period). The thickest lines are for the three days with NO_2 concentrations higher than 125 μg m^{-3} (the maximum concentration for each day is indicated in the legend and its exact time with a symbol in the time series). Vertical dashed line shows the approximate time of astronomical sunset. Measurements shown are from the sonic anemometer installed at the terrace. A moving average (smoothing) of 2 h has been applied to the time series for a better visualization, see Fig. 6a of the main article for the non-smoothed values. The same figure with the Street sonic is included in Fig. S8 of supplemental material.

Table 6
Mean wind speed (WS, in m s^{-1}), turbulent kinetic energy (TKE, in m^2 s^{-2}), and friction velocity (u_*, in m s^{-1}) during the afternoon (12:00 to 18:00 UTC) and evening (18:00 to 21:00 UTC) for each day of the stable period analysed. The maximum NO_2 concentration reached during each day is shown in the last raw (in μg m^{-3}), with the three days with highest concentration in bold. All measurements were obtained from the sonic installed at the terrace. The same table with measurements from the Street sonic is included in Table S6 of supplemental material.

	Day 19	Day 20	**Day 21**	**Day 22**	**Day 23**	Day 24
WS (afternoon)	1.15	1.25	1.05	0.93	0.96	1.54
WS (evening)	0.73	0.89	0.56	0.60	0.86	1.49
TKE (afternoon)	0.48	0.54	0.55	0.44	0.48	1.05
TKE (evening)	0.22	0.07	0.07	0.11	0.20	0.73
u$_*$ (afternoon)	0.25	0.27	0.35	0.32	0.34	0.49
u$_*$ (evening)	0.22	0.08	0.10	0.13	0.18	0.36
NO_2 (max)	112	119	**162**	**146**	**163**	107

The differences in turbulence between the sonics are illustrated in Fig. 9, which shows the MRFD of TKE for the Terrace sonic (left panel) and the Street sonic (right panel). The MRFD allows comparing the TKE contribution from each range of time scales, especially in the turbulent (smaller) scales (due to the higher resolution of MRDF in these scales). The time series of the NO_2 concentration is also included in the figures (white lines), as well as the total TKE (as the sum of the contribution from all scales up to 10 min, in black line). The three days show similar behaviour, with the afternoon turbulence diminishing at around 18:30 UTC, soon after the sunset, followed by a near-calm period that lasts until the arrival of the thermally-generated flows. This led to a clear increase in the turbulence levels at around 22:00 UTC, which coincides with the NO_2 reduction. However, some small-scale differences exist among the three days, especially in the features observed between 18:30 and 22:00 UTC, which is the calmer period of the evening, in which other *meso* and sub-meso processes typically gain importance (Mahrt, 2014). These differences are commented below:

Day 21 registered the minimum TKE value in the whole period (0.007 m^2 s^{-2} at the terrace level and 0.002 m s^{-1} at the street) at around 19:30 UTC, when the turbulence was suppressed at both levels. This calm period was followed by a gradual increase in turbulence and wind (Fig. 8) from 19:30 UTC to midnight, associated with a continuous NO_2 diminution. At the street level, the calm

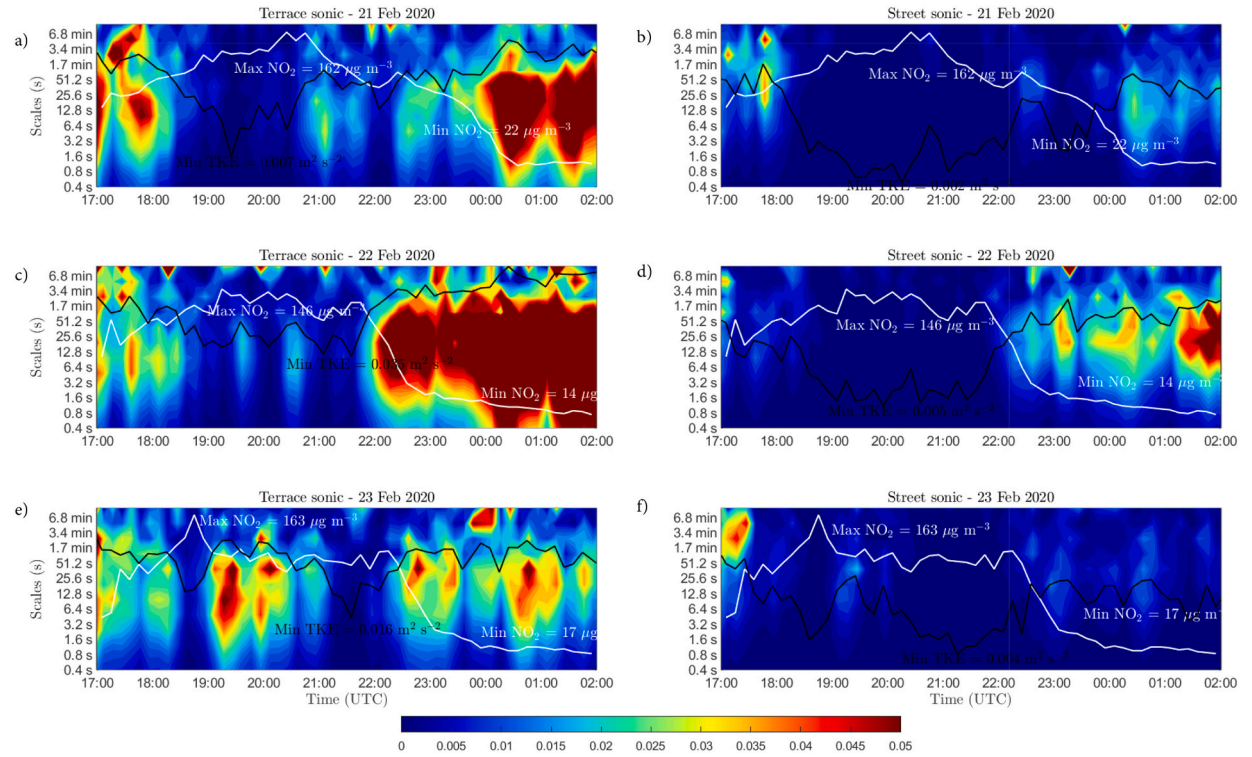

Fig. 9. Multi-resolution flux decomposition for the Turbulent Kinetic Energy (TKE) (m s^{-1}) for the three days with $NO_2 > 125$ μg m^{-3}: 21 of February 2020 (top panels), 22 of February 2020 (middle panels) and 23 February 2020 (bottom panels) using the Terrace sonic (left panels) and the Street sonic (right panels). The black line represents the total TKE (logarithmic scale from 0.002 to 1.3 m^2 s^{-2} in all the panels, not shown) and the white line displays the NO_2 concentration (linear scale from 0 to 170 μg m^{-3} in all the panels, not shown). Both lines are included to make easier the visualization of their relation with the MRFD contour graphic. The period represented comprises from 17:00 to 02:00 UTC of the following day, i.e., the afternoon/evening transition with the first hours of the night, including the period when thermally-driven winds are typically observed.

period was more intense, but the NO_2 concentration was very sensitive to the small increase of turbulence observed between 20:30 and 21:00 UTC (Fig. 9b). At the terrace, the scales associated with this small increase in turbulence presented turbulent features (Fig. 9a, scales up to 50 s at 21:00 UTC), somehow decoupled from the presence of motions with slightly larger scales of >3 min. However, at the street level (Fig. 9b), this increase in turbulence was more associated with the larger scales (i.e., the turbulent motions were not present), but this seemed enough to cause the NO_2 reduction. Indeed, these differences were also observed in the wind speed signal, which increased slightly at the terrace level but not at the street (Fig. 8 and Fig. S8 of the supplemental material). Afterwards, the wind speed and turbulence clearly increased progressively from 23:00 UTC onwards, with thermally-driven flows that established through the night and with NO_2 concentration that diminished up to 22 μg m^{-3}.

Day 22 was similar to the previous one, but with a calm period characterised by cyclic increases in turbulence from small scales well separated from larger ones (>7 min). This is very well observed from the MRFD figure of the TKE calculated from the Terrace sonic (Fig. 9c from 18:30 to 21:30 UTC). At the street level, however, the larger-scale signal was also observed but not the turbulent ones. However, these intermittent increases in turbulence were weaker than the one observed at 21:00 UTC and the NO_2 concentration remained high and relatively constant during this calm period, which remarks (somehow) the inefficient mixing of these large scales observed in the MRFD figures. Later, the thermally-driven wind arrived sharply around 21:30–22:00 UTC, increasing the turbulence and causing a quick decrease in NO_2 up to very small values (11 μg m^{-3}).

Day 23 displayed a sooner turbulent reduction (at all scales) around 18:30 UTC, with the maximum NO_2 concentration of the whole analysed time series. However, the calm period during this day was shorter due to the appearance of a wind system observed between 19:00 and 20:30 UTC (Fig. 8) which caused a marked increase in turbulence (Figs. 9e and f), leading to a quick NO_2 decrease. But the stabilization continued after this transient wind-speed increase and the NO_2 concentration remained relatively high until the arrival of the thermally-generated winds at the typical hours (around 22:00 UTC).

The evolution of the transient wind-speed increase at 19:00–20:30 UTC commented in the previous paragraph is illustrated with a red line in Fig. 8, as well as in the more detailed Fig. 10. Unlike for days 21 and 22, this wind speed increase during day 23 at 19:00 UTC does not seem linked to the typical formation of thermally-driven winds (Fig. 10b), which are normally associated with a drastic wind-direction change towards NNE (see typical behaviour in the blue line of Fig. 6a).

Besides, the turbulence-wind relationship was different between the later-formed thermally-driven flow and this transient event, which displayed more intense turbulence but lower wind speed than the NE wind observed at 22:00 UTC (stronger wind but weaker

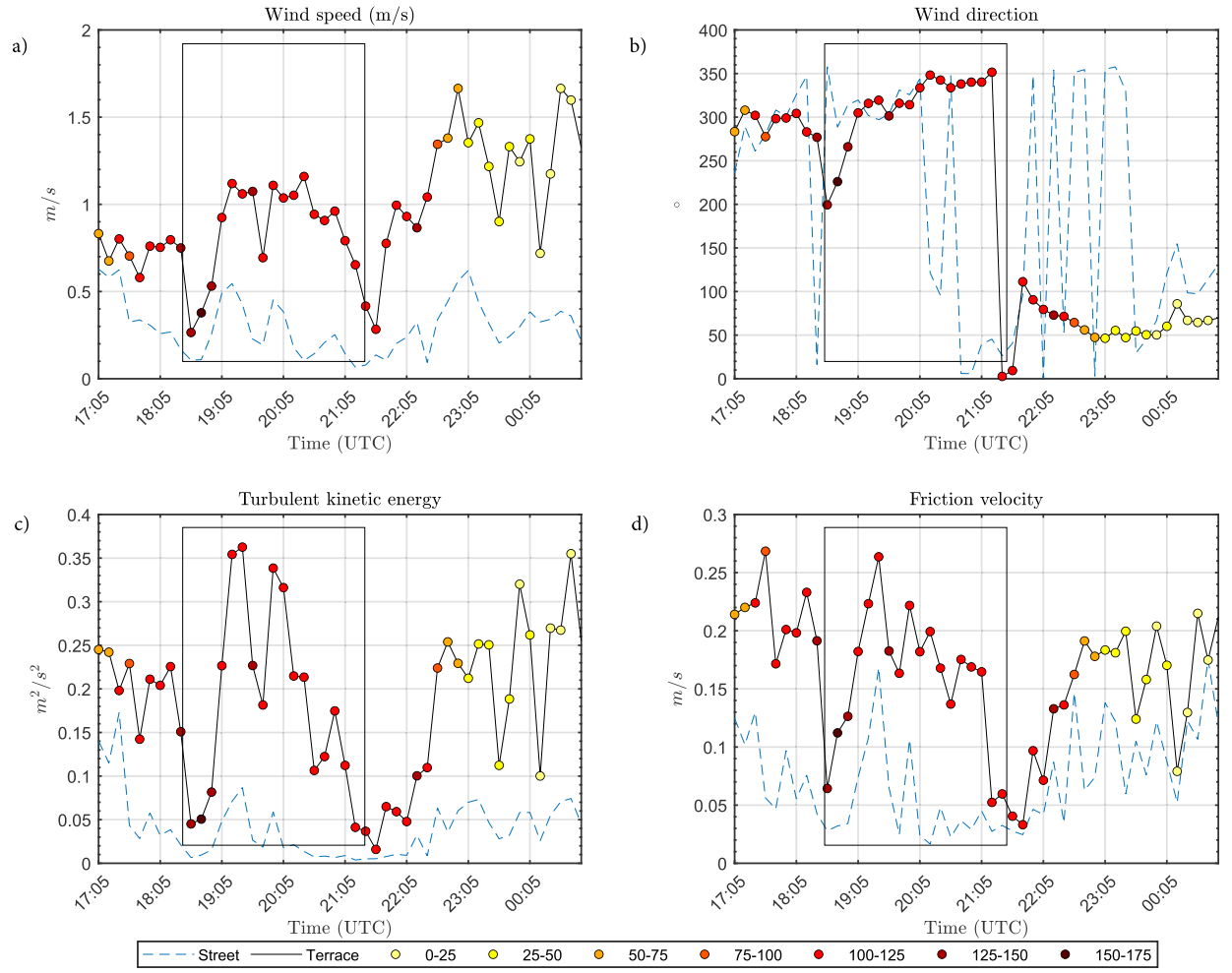

Fig. 10. Wind speed (a), wind direction (b), turbulent kinetic energy (c) and friction velocity (d) from 17:00 UTC of day 23 February to 01:00 UTC of day 24 February for the terrace (black line with symbols) and the street (blue dashed line) sonics. The symbols indicate the NO_2 concentration in $\mu g\ m^{-3}$. The black box indicates the unexpected wind and turbulence increase around 19:00 UTC. (For interpretation of the references to colour in this figure legend, the reader is referred to the web version of this article.)

turbulence, see Fig. 10, panels a, c and d).

This fact highlights the differences between the two wind systems in terms of wind (speed and direction) and associated turbulence, probably caused by their different vertical structure, affecting the wind shear and the vertical diffusive capacity of each one. Indeed, the decrease in NO_2 observed due to the short event analysed before was weaker than the effect of the thermally-driven wind observed the days 21, 22 and 23, which were more effective on the NO_2 reduction. Although this can be also affected by the different times of appearance of both wind systems, the wider range of eddy scales of the later-formed thermally-driven winds could help this diffusion.

4. Discussion about the study limitations

The analyses and conclusions that can be extracted from the previous results deserve different points of discussion.

4.1. Interpretation of the correlations

This work analyses correlations between wind/turbulence and NO_2 concentration. When these correlations are interpreted, in some cases we depart from the hypothesis that a better (more negative) correlation of NO_2 with some of the possible values of the meteorological variables (sonic emplacement and type of variable used) means a better representation of the real diffusion in the area. That is, in other words, we use the NO_2 concentration as a passive tracer of diffusion in the city. In this sense, both TKE and u_* have been calculated using the EC method, whose departing hypothesis are non-fulfilled in urban environments, especially for the measurements taken at the street level (more perturbed). However, the results suggest that even with these limitations, the high-frequency measurements taken at this level seem to be useful to calculate turbulent parameters.

4.2. Comparison among seasons

The comparisons done between sonics and variables for the same period are always performed with the same data sampling to allow fair comparisons (same background conditions, same emission, etc.). However, the comparison of the results among different seasons (or days) should be done with caution since the periods compared are different and cover a limited period with specific conditions. Hence, they can be affected by differences in the strength, duration and time of the emissions, affecting the NO_2 concentration. Other limitations include the different chemical reactivity of this pollutant depending on the season (or day) and even differences in the advection term from nearby sites under specific conditions.

4.3. Traffic intensity

The NO_2 concentration is logically also affected by the intensity of the emissions. In this context, it is remarkable that two of the three days with the highest concentrations were weekend days (the days 22 and 23 of February, see Fig. 6c), which are commonly associated with lower NO_2 concentration due to the decrease in traffic intensity. This fact indicates that the NO_2 concentration measured close to the surface in the cases here shown seems more modulated by the meteorological conditions than the traffic itself. The analysis of Fig. 6c shows how the hours with maxima NO_2 concentrations are always observed just after the secondary maxima in the traffic intensity associated with back-home driving during weekdays (Monday to Friday), i.e. when the traffic starts to decrease. In addition, the traffic intensity is high (around 2000 vehicles/h) during most of the daytime, not only at the morning and evening peaks. As commented before, this period of the day also coincides with the ABL stabilization due to the radiative cooling of the surface and subsequent inhibition of the turbulent vertical mixing. This is why the correlation of NO_2 with the traffic was in general low (see Fig. 3) despite the traffic being the main source of NO_2 emission in Madrid.

4.4. Site particularities

Finally, it is worth noting the particularities of the specific area here studied, which corresponds to a specific site in the city of Madrid. The extrapolation of the results to other cities and, even, to other sites in the city of Madrid, should be done with caution. On the one hand, the NO_2 measurements are close to a street with dense traffic (Castellana street) but can be also affected by some of the particularities of the specific location of the instruments. On the other hand, the same is applied to sonic anemometers, which can be more or less affected by the city obstacles depending on the wind direction, stability conditions, etc. All of these aspects are difficult to be controlled using real measurements. In this sense, more-intense field campaigns with a larger number of sonic anemometers would be necessary to further explore the microscale differences among the different parts in the city (both vertical and horizontal).

4.5. Turbulent scales involved in the NO_2 diffusion

The turbulent motions in the lower atmosphere are, by definition, composed of numerous eddies with different spatial scales. In this sense, the use of high-frequency raw sonic data allows the calculation of the contribution to the total flux, turbulent parameter, or covariance from each range of temporal scale through the harmonic analysis of the time series. As commented before, we have used the MRFD technique to focus on the smallest spatial scales that contribute to turbulence. It should be noted that the high-frequency measurements used to calculate turbulent parameters and fluxes through the eddy-covariance or MRFD methods are eulerian and do not allow directly calculating eddy sizes. However, the direct measurements are valid to estimate the time scales of the eddies that can be inferred from the time series analysis.

5. Summary and conclusions

This work presents a fine-scale analysis of the relationships found between the NO_2 concentration and the wind-turbulence measured from two sonic anemometers deployed in the city of Madrid during two field campaigns, which were developed in the frame of the AIRTEC-CM project. One of the sonic was installed very close to the street level, just above where the NO_2 was measured. The second one was installed in the same area but over the terrace of a tall building, less perturbed by city obstacles but farther from the NO_2 measurements at the surface. The overall objective of the work was to study the differences in the NO_2 -wind and NO_2 -turbulence, as well as to check if the results are conserved at both emplacements during different periods (summer, winter, and a stable period in winter), paying special attention to the micro and mesoscale meteorological phenomena that could affect the NO_2 evolution.

The NO_2 concentrations observed during the winter field campaign were notably larger than during the summer one. This expected result was attributed to the higher values of wind in summer, but, especially, to the enhanced turbulence during the daytime in summer, which favoured the NO_2 dispersion before the evening calm period, when the NO_2 maxima are typically observed in the city. Hence, the enhanced convection during the daytime in summer favoured low afternoon NO_2 concentration, which also affected the values reached during the evening transition and first hours of the night.

Although the correlations between NO_2 and wind or turbulence were similar, a slightly better relationship was found for the turbulent variables obtained from the sonic located closer to the street, especially for the friction velocity. This result was more evident during a winter stable period, characterised by high NO_2 concentrations during the evening, as also found in other studies (e.g., Yuval et al., 2020). This suggests that the information from the near-surface turbulence (including the vertical component of the flow) can

add valuable information for air-quality prediction purposes. It also indicates that the turbulence calculation at the street level is appropriate, despite the city obstacles around the area where the sonic was installed. The same result was not found when using data from the Terrace sonic, with slightly better (anti)correlation of NO_2 with wind speed (except in the stable period), which could indicate how the turbulence at the Terrace level was somehow de-coupled to the diffusion at the street level.

The comparison of the TKE, u*, and wind speed distributions for different NO_2 concentration ranges illustrate how the higher concentrations were associated with very low values of the meteorological variables. In an attempt to establish threshold values of these variables to be associated with high NO_2 concentration (higher than 125 $\mu g\ m^{-3}$), we calculated different performance scores. The results from this analysis showed how the meteorological variables calculated from the Street sonic exhibited a much better skill for this aim than the variables calculated using the Terrace sonic, especially the TKE at the street level.

Subsequently, the study focuses on the analysis of the synoptically stable period (19–24 Feb 2020), where the highest NO_2 concentrations were observed. The typical evolution of these days included the evening stabilization (decrease in turbulence and wind speed) after sunset, leading to the highest NO_2 concentrations. Conversely, these periods were also characterised by a quick and intense decrease in NO_2 concentration a few hours later due to the appearance of thermally-driven winds that were also favoured under stable conditions, leading to NO_2 concentrations that were lower than the ones observed during less-stable days. Hence, in this case, the complex topography (and heterogeneous terrain) acted towards the pollutant dispersion, unlike other cases in which the topography favours higher concentrations of pollutants (as happens in cities located in valleys).

Furthermore, from the comparison of the six days of the stable period, we demonstrated how the variability in the NO_2 maxima seemed related to the wind and turbulence values observed during the evening, but especially during the afternoon hours, as was also found during the summer field campaign. Despite that the days of this stable period showed a high correlation of NO_2 with wind and turbulence (in absolute values), the fine-scale analysis revealed how the correlations were also very sensitive to some local-mesoscale phenomena that cause short-lived and unexpected variations in wind speed and turbulence, affecting to the typical evolution of NO_2 and the correlations found. In this sense, the specific short-lived phenomena here analysed display some differences with other wind systems like the typical thermally-driven winds. These differences seemed associated with the characteristics of the wind systems, with short-lived events composed of smaller scales, weaker winds, and higher levels of turbulence. Although we highlight the possible local character of this wind system here analysed, it suggests the importance of the correct comprehension of the wind and turbulence fine-scale structure of the lower layers of the planetary boundary layer to also understand how they affect the pollutants dispersion.

CRedit authorship contribution statement

C. Román-Cascón: Conceptualization of this study, data preparation, scientific analysis, writing. **C. Yagüe:** Field campaign design, results interpretation, main project IP. **P. Ortiz-Corral:** Results interpretation, data calculation. **E. Serrano:** Results interpretation, synoptic analysis, text editing. **B. Sánchez:** Results discussion, text editing. **G. Maqueda:** Field campaign design. **G. Maqueda:** Field campaign design. **E. Alonso-Blanco:** Field campaign design, text editing. **B. Artiñano:** Field campaign design. **F.J. Gómez-Moreno:** Field campaign design. **E. Diaz-Ramiro:** Field campaign design. **J. Fernández:** Field campaign design. **A. Martilli:** Results discussion. **A. M. García:** Field campaign design, text editing. **A. Núñez:** Field campaign design, text editing. **J. M. Cordero:** Field campaign design. **A. Narros:** Field campaign design. **R. Borge:** Field campaign design, main project PI.

Declaration of Competing Interest

The authors declare that they have no known competing financial interests or personal relationships that could have appeared to influence the work reported in this paper.

Data availability

Data will be made available on request.

Acknowledgements

This work has been funded by the Madrid Autonomous Community and the European Commission (FSE) under the AIRTEC-CM (S2018/EMT4329) project. The Madrid City Council is specially acknowledged for its support for the experimental campaigns and data provided. CRC was funded by a IJC2020-043767-I Juan de La Cierva–Incorporación postdoctoral grant, funded by MCIN/AEI/10.13039/501100011033 and the Unión Europea NextGeneration EU/PRTR (during the last part of this work).

Appendix A. Supplementary data

Supplementary data to this article can be found online at https://doi.org/10.1016/j.uclim.2023.101663.

References

Barnes, L.R., Schultz, D.M., Gruntfest, E.C., Hayden, M.H., Benight, C.C., 2009. Corrigendum: false alarm rate or false alarm ratio? Weather Forecast. 24, 1452–1454. https://doi.org/10.1175/2009WAF2222300.1.

Bernardini, F., Trezzi, R., Quartesan, R., Attademo, L., 2020. Air pollutants and daily hospital admissions for psychiatric care: a review. Psychiatr. Serv. 71, 1270–1276. https://doi.org/10.1176/appi.ps.201800565.

Borge, R., Narros, A., Artñano, B., Yagüe, C., Gómez-Moreno, F.J., de la Paz, D., Román-Cascón, C., Díaz, E., Maqueda, G., Sastre, M., et al., 2016. Assessment of microscale spatio-temporal variation of air pollution at an urban hotspot in Madrid (Spain) through an extensive field campaign. Atmos. Environ. 140, 432–445.

Borge, R., Requia, W.J., Yagüe, C., Jhun, I., Koutrakis, P., 2019. Impact of weather changes on air quality and related mortality in Spain over a 25 year period [1993–2017]. Environ. Int. 133, 105272 https://doi.org/10.1016/j.envint.2019.105272.

Cordero, J.M., Núñez, A., García, A.M., Borge, R., 2021. Assessment and statistical modelling of airborne microorganisms in Madrid. Environ. Pollut. 269, 116124 https://doi.org/10.1016/j.envpol.2020.116124.

Donnelly, A., Misstear, B., Broderick, B., 2011. Application of nonparametric regression methods to study the relationship between no2 concentrations and local wind direction and speed at background sites. Sci. Total Environ. 409, 1134–1144. https://doi.org/10.1016/j.scitotenv.2010.12.001.

Fernando, H.J., Zajic, D., Di Sabatino, S., Dimitrova, R., Hedquist, B., Dallman, A., 2010. Flow, turbulence, and pollutant dispersion in urban atmospheres. Phys. Fluids 22, 051301. https://doi.org/10.1063/1.3407662.

Glencross, D.A., Ho, T.R., Camiña, N., Hawrylowicz, C.M., Pfeffer, P.E., 2020. Air pollution and its effects on the immune system. Free Radical Bio. Med. 151, 56–68. https://doi.org/10.1016/j.freeradbiomed.2020.01.179.

Grundström, M., Hak, C., Chen, D., Hallquist, M., Pleijel, H., 2015. Variation and co-variation of pm10, particle number concentration, nox and no2 in the urban air–relationships with wind speed, vertical temperature gradient and weather type. Atmos. Environ. 120, 317–327. https://doi.org/10.1016/j.atmosenv.2015.08.057.

Harlan, S.L., Ruddell, D.M., 2011. Climate change and health in cities: impacts of heat and air pollution and potential co-benefits from mitigation and adaptation. Curr. Opin. Environ. Sustain. 3, 126–134. https://doi.org/10.1016/j.cosust.2011.01.001.

Howell, J., Mahrt, L., 1997. Multiresolution flux decomposition. Bound.-Layer Meteorol. 83, 117–137. https://doi.org/10.1023/A:1000210427798.

Jhun, I., Coull, B.A., Schwartz, J., Hubbell, B., Koutrakis, P., 2015. The impact of weather changes on air quality and health in the United States in 1994–2012. Environ. Res. Lett. 10, 084009 https://doi.org/10.1088/1748-9326/10/8/084009.

Laña, I., Del Ser, J., Padró, A., Vélez, M., Casanova-Mateo, C., 2016. The role of local urban traffic and meteorological conditions in air pollution: a data-based case study in Madrid, Spain. Atmos. Environ. 145, 424–438. https://doi.org/10.1016/j.atmosenv.2016.09.052.

Lateb, M., Meroney, R.N., Yataghene, M., Fellouah, H., Saleh, F., Boufadel, M., 2016. On the use of numerical modelling for near-field pollutant dispersion in urban environments - a review. Environ. Pollut. 208, 271–283. https://doi.org/10.1016/j.envpol.2015.07.039.

Li, Z., Ming, T., Liu, S., Peng, C., de Richter, R., Li, W., Zhang, H., Wen, C.Y., 2021. Review on pollutant dispersion in urban areas-part A: effects of mechanical factors and urban morphology. Build. Environ. 190, 107534 https://doi.org/10.1016/j.buildenv.2020.107534.

Mahrt, L., 2014. Stably stratified atmospheric boundary layers. Annu. Rev. Fluid Mech. 46, 23–45. https://doi.org/10.1146/annurev-fluid-010313-141354.

Martilli, A., Sanchez, B., Rasilla, D., Pappaccogli, G., Allende, F., Martin, F., Román-Cascón, C., Yagüe, C., Fernandez, F., 2021. Simulating the meteorology during persistent wintertime thermal inversions over urban areas. The case of Madrid. Atmos. Res. 263, 105789 https://doi.org/10.1016/j.atmosres.2021.105789.

Mayer, H., 1999. Air pollution in cities. Atmos. Environ. 33, 4029–4037. https://doi.org/10.1016/S1352-2310(99)00144-2.

Patra, A., Colvile, R., Arnold, S., Bowen, E., Shallcross, D., Martin, D., Price, C., Tate, J., ApSimon, H., Robins, A., 2008. On street observations of particulate matter movement and dispersion due to traffic on an urban road. Atmos. Environ. 42, 3911–3926. https://doi.org/10.1016/j.atmosenv.2006.10.070.

Querol, X., Alastuey, A., Pandolfi, M., Reche, C., Perez, N., Minguillón, M.C., Moreno, T., Viana, M., Escudero, M., Orio, A., et al., 2014. 2001–2012 trends on air quality in Spain. Sci. Total Environ. 490, 957–969. https://doi.org/10.1016/j.scitotenv.2014.05.074.

Raaschou-Nielsen, O., Andersen, Z.J., Beelen, R., Samoli, E., Stafoggia, M., Weinmayr, G., Hoffmann, B., Fischer, P., Nieuwenhuijsen, M.J., Brunekreef, B., et al., 2013. Air pollution and lung cancer incidence in 17 european cohorts: prospective analyses from the european study of cohorts for air pollution effects (escape). Lancet Oncol. 14, 813–822. https://doi.org/10.1016/S1470-2045(13)70279-1.

Rajagopalan, S., Al-Kindi, S.G., Brook, R.D., 2018. Air pollution and cardiovascular disease: JACC state-of-the-art review. J. Am. Coll. Cardiol. 72, 2054–2070. https://doi.org/10.1016/j.jacc.2018.07.099.

Román-Cascón, C., Steeneveld, G., Yagüe, C., Sastre, M., Arrillaga, J., Maqueda, G., 2016. Forecasting radiation fog at climatologically contrasting sites: evaluation of statistical methods and WRF. Q. J. Roy. Meteor. Soc. 142, 1048–1063. https://doi.org/10.1002/qj.2708.

Santiago, J., Sanchez, B., Quaassdorff, C., de la Paz, D., Martilli, A., Martín, F., Borge, R., Rivas, E., Gómez-Moreno, F., Díaz, E., et al., 2020. Performance evaluation of a multiscale modelling system applied to particulate matter dispersion in a real traffic hot spot in Madrid (Spain). Atmos. Pollut. Res. 11, 141–155. https://doi.org/10.1016/j.apr.2019.10.001.

Schaefer, J.T., 1990. The critical success index as an indicator of warning skill. Weather Forecast. 5, 570–575. https://doi.org/10.1175/1520-0434(1990)005<0570:TCSIAA>2.0.CO;2.

Stull, R.B., 1988. An Introduction to Boundary Layer Meteorology, vol. 13. Springer Science & Business Media. https://doi.org/10.1007/978-94-009-3027-8.

Vilà-Guerau De Arellano, J., Duynkerke, P.G., 1992. Influence of chemistry on the flux-gradient relationships for the no-o3-no2 system. Bound.-Layer Meteorol. 61, 375–387. https://doi.org/10.1007/BF00119098.

Westervelt, D., Horowitz, L., Naik, V., Tai, A., Fiore, A., Mauzerall, D.L., 2016. Quantifying pm2. 5-meteorology sensitivities in a global climate model. Atmos. Environ. 142, 43–56. https://doi.org/10.1016/j.atmosenv.2016.07.040.

WHO, 2021. WHO Global Air Quality Guidelines: Particulate Matter (PM2. 5 and PM10), Ozone, Nitrogen Dioxide, Sulfur Dioxide and Carbon Monoxide: Executive Summary. World Health Organization.

Yuval, Tritscher T., Raz, R., Levi, Y., Levy, I., Broday, D.M., 2020. Emissions vs. turbulence and atmospheric stability: a study of their relative importance in determining air pollutant concentrations. Sci. Total Environ. 733, 139300 https://doi.org/10.1016/j.scitotenv.2020.139300.